

Site-specific local structure of Mn in artificial manganese ferrite filmsE. Kravtsov,^{1,2} D. Haskel,¹ A. Cady,¹ A. Yang,³ C. Vittoria,³ X. Zuo,⁴ and V. G. Harris³¹*Advanced Photon Source, Argonne National Laboratory, Argonne, Illinois 60439, USA*²*Institute of Metal Physics, Ekaterinburg 620041, Russia*³*Department of Electrical and Computer Engineering, Northeastern University, Boston, Massachusetts 02115, USA*⁴*College of Information Technical Science, Nankai University, Tianjin 300071, China*

(Received 10 May 2006; revised manuscript received 21 July 2006; published 25 September 2006)

Diffraction anomalous fine structure (DAFS) spectroscopy has been applied to resolve site-specific Mn local structure in manganese ferrite films grown under nonequilibrium conditions. The DAFS spectra were measured at a number of Bragg reflections in the vicinity of the Mn absorption K edge. The DAFS data analysis done with an iterative Kramers-Krönig algorithm made it possible to solve separately the local structure around crystallographically inequivalent Mn sites in the unit cell with nominal octahedral and tetrahedral coordination. The strong preference for Mn to be tetrahedrally coordinated in this compound is not only manifested in the relative site occupancies but also in a strong reduction in coordination number for Mn ions at nominal octahedral sites.

DOI: [10.1103/PhysRevB.74.104114](https://doi.org/10.1103/PhysRevB.74.104114)

PACS number(s): 61.10.Ht, 61.10.Nz, 75.50.Gg

I. INTRODUCTION

There has been considerable long-term interest in spinel ferrite materials due to their significant technological potential in high-frequency and magnetic recording applications. In particular, manganese ferrite (MnFe_2O_4) has attracted much attention and is widely used in electronics.¹⁻³ It is well established that the magnetic behavior of manganese ferrite (MFO) is closely tied to its structural properties. MFO has the same atomic structure as the mineral spinel, MgAl_2O_4 ($Fd\bar{3}m$ space group, No. 227 in the International Tables.⁴) The spinel unit cell consists of a pseudocubic close packing (ccp) of 32 oxygen anions surrounded by 96 interstices, with 24 interstices being occupied by metallic cations.⁵ MFO adopts a mixed spinel structure where Mn and Fe ions are distributed between 8 tetrahedral and 16 octahedral interstitial sites in the unit cell. In the following, we refer to the tetrahedral sites as A sites and the octahedral ones as B sites. Generally, Mn atoms prefer to occupy A sites in the unit cell, but there is a small fraction of Mn atoms at B sites. A typical MFO sample prepared with conventional equilibrium growth techniques³ contains about 20% Mn ions in octahedral sites and 80% Mn ions in tetrahedral sites.

Modern deposition techniques allow the site-occupancy ratio in ferrites to be varied to a large extent by utilizing nonequilibrium growth conditions. For example, the possibility to manipulate site occupancies in MFOs by using a newly developed alternating target laser ablation deposition (ATLAD)^{6,7} was demonstrated. This technique has been shown to produce ferrite films having enhanced anisotropy fields by adjusting the cation distribution far from equilibrium by means of an atomic layer-by-layer growth. These ferrites have been referred to in the scientific literature as “artificial” ferrites.⁸ The close connection between structural and magnetic properties of ferrites has been appreciated for many years,² and much effort has been made toward developing methods for structural investigation of ferrites. It is worth pointing out that the structural analysis is often limited to consideration of cation distribution between crystallo-

graphically inequivalent sites with only a small emphasis placed on the local structural environment around these sites. To go along with recent advances in growth techniques, the need for precise local structure determination in ferrite studies becomes more apparent.

While site occupancy is one of the most important structural parameters, being able to tune properties of these new artificial structures requires additional site-specific information such as cation valences, coordination numbers, and bond distances. We report here on the application of diffraction anomalous fine structure (DAFS) spectroscopy to structural studies of artificial MFO films. We show that this method allows us to resolve site-specific Mn local structure in these films. We prove the validity of our results through self-consistent analysis of site-specific data obtained in the diffraction channel, and site-averaged data obtained in the absorption channel. We demonstrate that DAFS spectroscopy is able to resolve local atomic environment of Mn atoms in A and B sites. Finally, we provide possible reasons for the observed reduction in the coordination number at B sites and the expansion of cation-oxygen distance at A sites.

II. DAFS TECHNIQUE

A good number of experimental methods exist to probe the local structure in ferrites, like Mössbauer spectroscopy (see, for example, Ref. 9 and references therein), pair distribution function analysis of x-ray and neutron scattering,¹⁰ and extended x-ray absorption fine structure (EXAFS) spectroscopy. EXAFS spectroscopy is widely recognized as a powerful tool for the determination of local atomic structure in materials.^{11,12} This technique is readily applied in investigations of materials containing a single absorbing site. However, for spinel ferrites, where absorbing atoms reside in two crystallographically inequivalent sites, the ability of EXAFS to independently refine the local structure around these sites is reduced due to the necessity to refine overlapping signals from these sites. In the particular case of manganese ferrites, the spatial resolution in EXAFS is limited by the difference

between Mn (6539 eV) and Fe (7112 eV) *K*-edge energies, which limits the Mn EXAFS to a maximum photoelectron wave number $k_{max} \sim 10 \text{ \AA}^{-1}$. The spatial resolution δr available in EXAFS is then estimated as $\pi/2k_{max} \geq 0.15 \text{ \AA}$. As discussed below, this is not enough to resolve contributions from different crystallographic sites.

DAFS spectroscopy^{13,14} is an ideal tool to probe site-specific Mn local structure in manganese ferrites. This technique implies measuring the energy dependence of the diffracted intensity at different Bragg peaks. By choosing a proper set of Bragg reflections, it is possible to separate completely the contributions from crystallographically inequivalent sites providing EXAFS-like information for each site separately. The problem of overlapping signals is mitigated and the local structure for each site can be completely determined. Despite the potential merits of DAFS, this technique has not been used to study crystallographically inequivalent sites in manganese spinel ferrite materials. Its application to a more common class of spinel ferrites is limited to a few attempts to look at charge ordering by measuring forbidden Bragg reflections without much consideration for the fine structure (see Ref. 15 and references therein). One exception is the work of Frenkel *et al.*¹⁶ who applied DAFS to resolve Fe local structure in magnetite. Unfortunately, this research was limited to the octahedrally coordinated (B) sites only.

In general, DAFS experimental procedures and data-treatment principles have been elaborated in the literature,^{14,17–21} but practical aspects of DAFS data analysis are still under discussion. One approach is to extract structural information by direct fitting of experimental DAFS spectra.²² This approach has been successfully applied to some systems but, as discussed below, in our particular case the direct fitting is very difficult to perform. A more common strategy in DAFS data treatment is to reduce measured DAFS spectra to EXAFS-like data sets for isolated crystallographically inequivalent sites. If this step is done, the analysis can proceed with well-established EXAFS methods using theoretical standards. This first step in data reduction, however, has generated significant debate.²³ While several methods were suggested for this procedure, it was argued²³ that some methods might introduce systematic errors in the refined data, and presently there is no consensus concerning reliability criteria for the refinement procedure. In the present paper we prove the reliability of our analysis procedures by performing a number of self-consistency checks. First, we compare the fine structure associated with A sites as derived from two independent sets of Bragg reflections. Second, the EXAFS spectrum measured in fluorescence geometry is compared with the site-averaged spectrum calculated using site-specific parameters provided by DAFS analysis.

III. DAFS ANALYSIS PROCEDURE

The main principles of DAFS data analysis are well known. Here we describe only common details essential for our consideration and refer the interested reader to the literature.^{14,18–21} We start from the energy-dependent crystallographic structure factor that can be written at a given wave vector \mathbf{Q} as a sum of nonresonant and resonant contributions

$$F(\mathbf{Q}, E) = F_0 \exp(i\varphi) + \sum N_j \exp(i\mathbf{Q}\mathbf{R}_j) f_j(E). \quad (1)$$

The first term includes contributions to the structure factor coming from summing over non-resonant atoms (Fe and O) and Thomson scattering from resonant (Mn) atoms. Its concrete form is not important to us, we stress only that it is a complex term, linearly dependent on energy. This is not true on approaching the Fe *K* edge and for this reason we had to restrict our analysis to the energies well below the Fe absorption edge of 7112 eV. The second term describes resonant contributions from Mn atoms, with N_j being Mn site occupancies and $f_j(E) = f'_j(E) + if''_j(E)$ complex resonant scattering amplitudes that are different for crystallographically inequivalent Mn sites. By choosing different Bragg reflections, one can obtain contributions from A and B sites in different proportions. For our study, we selected (422), (222), and (111) Bragg reflections. By measuring the first two reflections, we separate Mn local structure around A and B sites, respectively, and the third measurement is useful to check self-consistency of the refinement procedure and to verify site occupancies for Mn cations. The crystallographic structure factor for these reflections has the following form:

$$F_{422} = f_{\text{Th}} + 8(1 - N_A)f_{\text{Fe}}(E) + 8N_A f_A(E), \quad (2)$$

$$F_{222} = f_{\text{Th}} - 32f_{\text{O}}(E) + 16(2 - N_B)f_{\text{Fe}}(E) + 16N_B f_B(E), \quad (3)$$

$$F_{111} = f_{\text{Th}} + [8(2 - N_B) - 4\sqrt{2}(1 - N_A)]f_{\text{Fe}}(E) + 8N_B f_B(E) - 4\sqrt{2}N_A f_A(E), \quad (4)$$

where f_{Th} is the sum of Thomson scattering terms for O, Fe, and Mn atoms, $f_{\text{Fe}}(f_{\text{O}})$ is scattering amplitude for nonresonant Fe(O) atoms, and $f_A(f_B)$ stands for scattering amplitude for resonant Mn atoms located at A(B) sites. Finally, by separating resonant and nonresonant contributions into the crystallographic structure factor, we write the theoretical intensity of the DAFS signal as follows:

$$I(E) \sim [F_0 \cos(\varphi) + f'_{hkl}(E)]^2 + [F_0 \sin(\varphi) + f''_{hkl}(E)]^2, \quad (5)$$

where $f'_{hkl}(E)$ and $f''_{hkl}(E)$ are real and imaginary parts of the resonant contributions into the structure factor for different reflections [Eqs. (2)–(4)].

In order to compare the calculated and experimentally measured DAFS intensity, one needs to account for experimental correction factors. Finally, the total calculated scattered intensity $I_T(E)$ can be written in the following form:

$$I_T(E) = I_{bgd}(E) + CA(\mathbf{Q}, E)L(\mathbf{Q}, E)P(\mathbf{Q}, E)I(E), \quad (6)$$

where C is a scaling factor, A , L , and P are the absorption, Lorentz, and polarization factor corrections, respectively. The background intensity is $I_{bgd}(E)$, generally approximated by a smooth polynomial function of second or third order. In case of a thin film of thickness t , the absorption correction is calculated as follows:²⁴

$$A(\mathbf{Q}, E) = \left[1 - \exp\left(-\frac{2\mu(E)t}{\sin(\theta)\sin(\chi)}\right) \right] / \frac{2\mu(E)}{\sin(\theta)\sin(\chi)}, \quad (7)$$

where $\mu(E)$ is the absorption coefficient, θ is the incidence angle, and χ is the tilt angle of the sample goniometer. In our data processing, we used the experimentally measured absorption coefficient, which was background subtracted and normalized using tabulated absorption cross sections. The polarization correction is given by the formula

$$P(\mathbf{Q}, E) = [(1 + \varphi) + (1 - \varphi)\cos^2(2\theta)]/2, \quad (8)$$

with φ being the degree of linear polarization of the beam, and the Lorentz factor is equal to

$$L(\mathbf{Q}, E) = 1/[E^3 \sin(2\theta)]. \quad (9)$$

DAFS data analysis can be done either by direct fitting of experimental DAFS spectra or with a more sophisticated method implying additional processing of the DAFS data. Direct fitting of DAFS spectra can be done only if one can neglect the quadratic terms in $f'_{hkl}(E)$ and $f''_{hkl}(E)$ in Eq. (5). This limitation of the direct fitting method has been discussed in the DAFS literature in some detail.²² Before having proceeded with our data analysis, we checked directly this condition for our particular system and selected Bragg reflections and found that there are energies for which the quadratic terms cannot be neglected. So direct fitting methods cannot be applied to our system and we had to use a more common approach. As discussed above, in this case quantitative analysis of DAFS data requires reduction to EXAFS-like spectra, i.e., refinement of the imaginary part of the resonant scattering amplitude $f''(E)$ from the quadratic expression for $f'_{hkl}(E)$ and $f''_{hkl}(E)$ in Eq. (5). In our DAFS data analysis, we used a refinement procedure based on the iterative Kramers-Krönig algorithm first suggested by Pickering *et al.*¹⁷ and further developed by Cross.²⁵ The procedure is based on the fact that the real and imaginary parts of the resonant scattering amplitude are related by the Kramers-Krönig relations:

$$f'(E) = \frac{2}{\pi} \int_0^\infty \frac{f''(\epsilon)\epsilon}{E^2 - \epsilon^2} d\epsilon, \quad (10)$$

$$f''(E) = -\frac{2E}{\pi} \int_0^\infty \frac{f'(\epsilon)}{E^2 - \epsilon^2} d\epsilon. \quad (11)$$

The refinement is done as follows: First, we start from a guess DAFS function constructed with the theoretical structure factor calculated by using tabulated values of $f'(E)$ and $f''(E)$.³⁰ Next, energy-independent parameters in Eqs. (5) and (6) are found by minimizing the difference between the experimental data and trial DAFS functions. With these parameters obtained, we refine $f'(E)$ from the DAFS equation and calculate new values of $f''(E)$ from the Kramers-Krönig transform. This is done iteratively, until the difference between old and new values of $f'(E)$ and $f''(E)$ becomes less than 10^{-5} . As a result of the refinement procedure, one obtains Kramers-Krönig related $f'(E)$ and $f''(E)$ as well as a set

of energy-independent fitting parameters that allow one to describe the experimental spectra. In order to check the uniqueness of the results obtained, we did additional tests as discussed below.

IV. EXPERIMENTAL

MnFe₂O₄ films were alternately ablated from two binary oxide targets (i.e., MnO and Fe₂O₃) allowing for atomic control of local chemistry and structure.²⁶ The thickness of each layer was controlled by adjusting the laser energy and the number of laser pulses incident upon the targets (KrF excimer laser at 248 nm; 400 mJ per pulse). The ratio of MnO to Fe₂O₃ laser shots was 4:10 resulting in magnetization values most closely matching the bulk. The calibration runs measured one laser pulse at this energy to correspond to a thickness of 0.4 ± 0.1 Å. The total film thickness was about $0.7 \mu\text{m}$. The oxygen pressure was 1 mtorr in depositions on (111) MgO single crystal substrates. Twice the lattice constant of MgO, $a_{\text{MgO}} = 4.216$ Å,^{27,28} nearly matches that of MnFe₂O₄, $a_{\text{MnFe}_2\text{O}_4} = 8.511$ Å,²⁹ resulting in a lattice mismatch of 0.94%. The thermal expansion coefficients, $\delta_{\text{MgO}} = 1.26 \times 10^{-5}/\text{K}$ (Ref. 27) and $\delta_{\text{MnFe}_2\text{O}_4} = 1.2 \times 10^{-5}/\text{K}$ (Ref. 27), are within 5%, resulting in little strain in the ablated films. The temperature of the substrate during deposition was held fixed at 700 °C. The EXAFS measurements⁷ have revealed Mn occupation of B sites to be $18 \pm 4\%$, which is close to the reported bulk value of 20%.³ This EXAFS analysis was done by constraining the coordination numbers to their nominal values. Details of the sample preparation and characterization are described elsewhere.^{6,7}

The DAFS measurements were done at undulator beamline 4-ID-D of the Advanced Photon Source (APS) at Argonne National Laboratory. The DAFS scans were done by tuning the x-ray energy with a double-crystal Si(111) monochromator while maintaining the sample diffraction condition (fixed Q). Toroidal and flat mirrors were used for focusing the undulator beam ($200 \times 150 \mu\text{m}$) and for harmonic rejection. The DAFS data were collected by measuring the diffracted peak intensity with a fast avalanche photodiode (APD) detector having a 5 nsec time resolution. With the APS ring filled with 324 bunches (11 nsec spacing) and a count rate on the diffracted beam of approximately 2×10^6 cts/sec, negligible detector dead-time was measured. Energy scans of the (111), (222), and (422) reflections were performed at room temperature within the energy range 6300–6900 eV, which includes the K -absorption edge of Mn at 6539 eV. The first two scans were done in standard $\theta-2\theta$ reflection geometry, whereas the last scan was done in an asymmetric geometry with the tilt angle of the sample χ approximately 60 degrees. Since magnetic measurements were attempted in the same experiment, a circularly polarized beam was used, with helicity-dependent spectra being detected with a digital lock-in technique.³¹ The measured spectra were averaged over two opposite helicities. Energy calibration was done by monitoring an absorption signal in a reference Mn foil. In order to provide proper absorption corrections of the DAFS signal and to check reliability of DAFS data analysis, EXAFS spectra were collected. The EXAFS

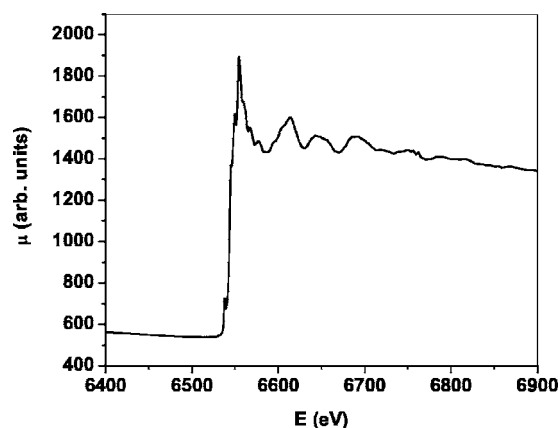


FIG. 1. Fluorescence EXAFS spectrum from MnFe_2O_4 artificial film normalized using tabulated absorption cross sections to provide the proper ratio of resonant and nonresonant contributions to the absorption coefficient. These data were used for absorption correction in the refinement of DAFS spectra as discussed in the text.

was measured in fluorescence geometry with an energy-dispersive Si-drift diode detector. Elastic background was rejected by Cr filters placed in front of the detector. Figure 1 shows the EXAFS spectrum from an MnFe_2O_4 artificial film measured around the Mn K edge, the background subtracted and normalized to tabulated values in order to provide the proper ratio of resonant and nonresonant contributions. Figure 2 shows raw DAFS spectra measured at the (422), (222), and (111) Bragg reflections through the Mn (6539 eV) absorption edge. As discussed above, the first scan (2a) probed A sites, the second one (2b)—B sites, and the last scan (2c) probed the difference between contributions from A and B sites taken with different weights according to Eq. (4), with the contribution from A sites dominating ($N_A \gg N_B$). Since resonant contributions to DAFS depend on site occupancies, we observe strong resonant signal coming from A sites [Figs. 2(a) and 2(c)] and much weaker signal from B sites (Fig. 2(b)). As can be seen in Fig. 2(b), resonant contribution from B sites becomes negligible at higher energies ($E \geq 6700$ eV) as compared with the background signal. For this reason, in our processing of the data in Fig. 2(b), we decided to restrict our analysis to the energy region below 6750 eV.

V. RESULTS

As an essential feature of the DAFS spectra (Fig. 2), we mention the appearance of a pre-edge peak near the Mn K -edge energy about 6539 eV. This feature is typical of tetrahedrally coordinated (A-site) manganese.^{32,33} This peak is rather strong for the Fig. 2(a) and Fig. 2(c) scans but weak for the Fig. 2(b) one. A similar pre-edge peak in the XANES spectrum (Fig. 1) is associated with the electronic transition from $1s$ core level to empty $3d$ states.^{32,33} This peak is a signature of a noncentrosymmetric local environment, since the dipole-forbidden $1s \rightarrow 3d$ transition becomes possible in this geometry due to p - d mixing. The existence of the strong pre-edge peak for A sites is consistent with our knowledge of

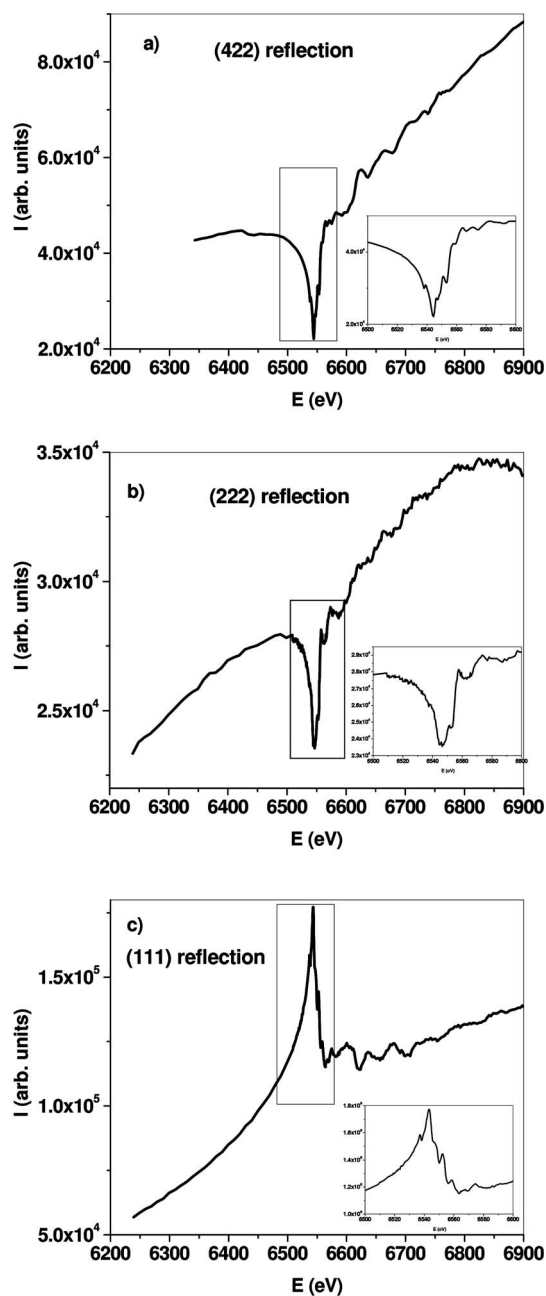


FIG. 2. Raw DAFS spectra of MnFe_2O_4 film obtained from Bragg reflections probing different site contributions: (a) purely A-site contribution measured at (422) reflection, (b) purely B-site contribution taken at (222) reflection, and (c) mixed contribution from both A and B sites measured at (111) reflections. The mixing ratio is discussed in the text.

their tetrahedral coordination. As for the B sites, the pre-edge peak is less intense but still present.

Figure 3(a) shows $f''(E)E \propto \mu(E)$ of Mn atoms located at A and B sites obtained from the refinement of the (422) and (222) DAFS signals. We note the presence of a shoulder at 6539 eV for tetrahedrally coordinated A sites, where the pre-edge peak appears in the absorption spectrum. In the figure one can also see a weak pre-edge peak for octahedrally coordinated B sites that is generally associated either with a

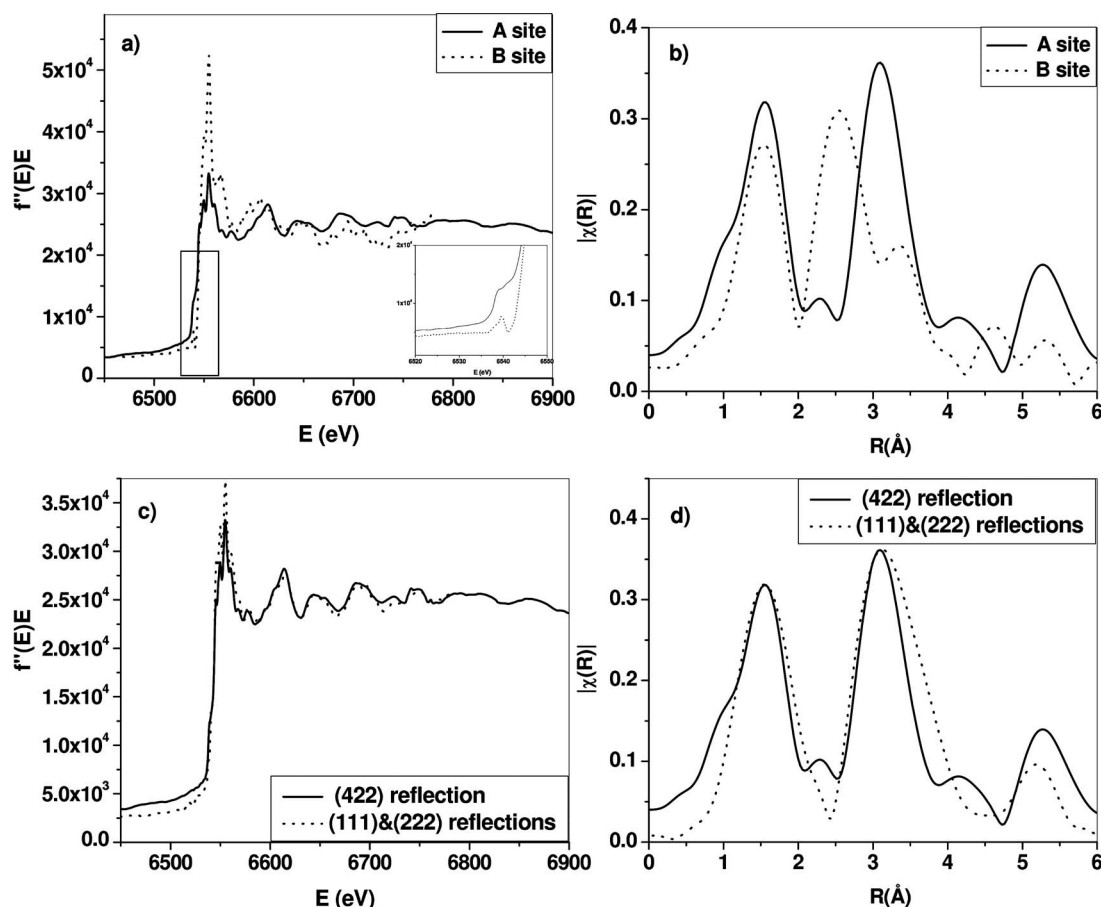


FIG. 3. (a) $f''(E)E \propto \mu(E)$ for Mn atoms located at A and B sites obtained from DAFS data refinement and (b) the magnitude of its complex Fourier transform. (c) $f''(E)E \propto \mu(E)$ for A sites calculated in two independent ways: directly from (422) DAFS spectrum (line) and by combining refinement results for (111) and (222) reflections (dashed line), and (d) the magnitude of the corresponding complex Fourier transform.

quadrupole electronic transition or with a distortion of local octahedral environment.³⁴ The data of Fig. 3(a) was background subtracted, reduced to photoelectron wave-vector space, and Fourier transformed to radial coordinates by using the Athena program code.³⁵ Fourier transforms were performed using a Hanning window over the k range 2.5–8.0 \AA^{-1} with a k weight of 1. Figure 3(b) shows the magnitude of the complex Fourier transform of the refined data for A and B sites.

In order to check the self-consistency of the refinement procedure, we also calculated $\mu(E)$ for A sites in a different way, i.e., by combining site-specific $f''(E)E$ derived from (111) and (222) Bragg signals and using the conditions in Eq. (4) with site occupancies $N_A=0.82$ and $N_B=0.18$ obtained from previous EXAFS analysis on the same film.⁷ The comparison is presented in Figs. 3(c) and 3(d). One can see that the refined spectra are very similar throughout the EXAFS region. Some misfit in the near-edge region can be explained by extra error introduced by combining two data sets. It is important to note that the two refinements of the A-site fine structure are totally independent from each other. First, we used the highly asymmetric (422) Bragg reflection that isolates the A sites but requires a more complicated self-absorption correction shown in Eq. (7). Second, we used

(111) and (222) Bragg reflections measured in reflection geometry. The two different procedures lead to similar results, and hence we can conclude that the refinement procedure is reliable and its results unique, i.e., they do not depend on the choice of particular Bragg reflection and scattering geometry.

Further analysis of the refined absorption spectra was done using EXAFS methods based on theoretical standards. Data fitting was done in R space using the Artemis program,³⁵ with theoretical standards generated by FEFF6 code.³⁶ Only the first two nearest neighbor shells were included in the fitting: Mn(A)-O, Mn(A)-Fe(B) for the A site and Mn(B)-O, Mn(B)-Fe(B) for the B site. In all cases, the adjusted parameters were a global S_0^2 and energy shift ΔE_0 , and bond distances R and mean squared disorder (MSD) σ^2 for every shell. The MnFe_2O_4 lattice parameter was determined by x-ray diffraction and fixed at 8.508 \AA .

Figure 4 shows the amplitude of the complex Fourier transform and the back Fourier transform to k space (denoted as q space) of the first two shells region for the A sites together with the corresponding fits to the data. The fitting results for bond distances R and MSDs are summarized in Table I. The first and second shell coordination numbers N were fixed during the fit. The passive electron amplitude reduction factor was found to be $S_0^2=0.84\pm 0.18$. Of the results of Table I we note an essential increase in the average A-O

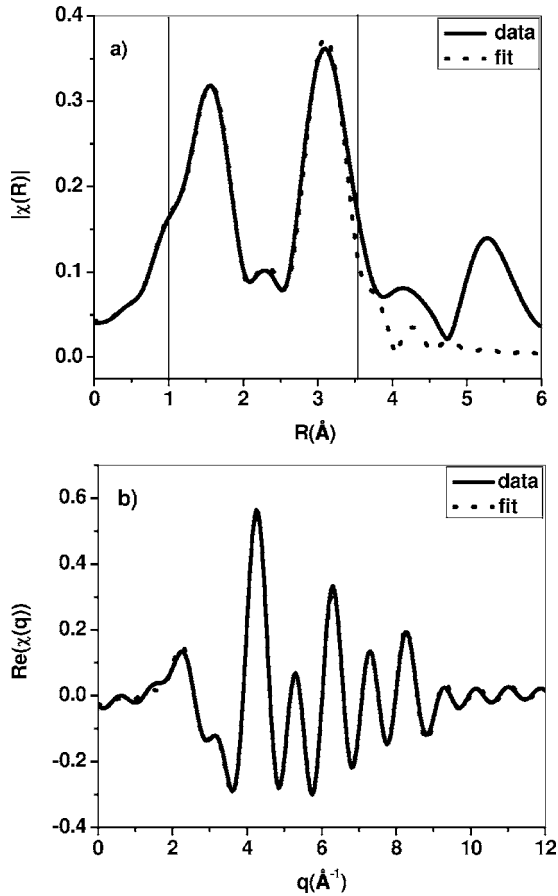


FIG. 4. (a) Magnitude of the complex Fourier transform of refined absorption data and its fit with FEFF6 theory for Mn absorbing atoms located at A sites. Vertical lines indicate fitting range. (b) Back Fourier transform of the fitted regions of R space and corresponding fit for Mn absorbing atoms located at A sites.

bond distance from 1.91 to 2.04 Å. The A-B bond distance also increases from 3.52 to 3.58 Å, which is in reasonable agreement with the value of 3.54 Å reported by Subías *et al.*³⁷ for the corresponding Fe(B)-Mn(A) distance in a bulk MnFe_2O_4 polycrystal.

The EXAFS of the Mn B-sites could not be fitted without varying coordination numbers from their nominal values. To fit the B-site EXAFS spectrum, we fixed the value of $S_0^2 = 0.84$ and allowed first and second shell coordination numbers N to vary. In order to determine true coordination numbers N , when there is a strong correlation between N and σ^2 parameters, the following procedure was used. Several data sets were prepared by Fourier transforming the refined experimental spectrum with different k weights as further explained in Ref. 38. Each data set was fitted with fixed param-

TABLE I. Best-fit structural parameters for the A site in MnFe_2O_4 artificial films obtained by fitting refined DAFS data.

Bond	N	R (Å)	σ^2 (10^{-3} Å ²)
A-O	4	2.04 ± 0.02	3.5 ± 1.0
A-B	12	3.58 ± 0.02	3.6 ± 1.0

eters σ^2 in the range 0.0005–0.02 Å² while the coordination number was allowed to vary. Coordination numbers and σ^2 were determined by assuming that they should not depend on the particular choice of the k weight for the Fourier transform. The fitting results thus obtained are listed in Table II. The amplitude of the complex Fourier transform and the back Fourier transform to q space of the two first shells region for the B site together with corresponding fits to the data are shown in Fig. 5. Except for the coordination numbers, the results of Table II are in good agreement with expectations.³⁷ The oxygen parameter u estimated from data of Tables I and II is equal to 0.386 for our film, which is close to the reported value of 0.385 for bulk MnFe_2O_4 crystals.² We note that forcing the first shell coordination number for B sites to be six leads to a physically unrealistic value of the passive electron amplitude reduction factor $S_0^2 = 0.43$. It is inconsistent with our knowledge that this factor be dependent on the absorbing atom only but not on the site occupied.

To further check the refinements and data treatment procedure, we did an additional test and checked if the measured fluorescence EXAFS spectrum of Fig. 1 could be reproduced with site-specific structural parameters provided by DAFS. For this purpose, the EXAFS spectrum was processed and Fourier transformed according to the same procedure as described above. The EXAFS data were fitted using the same theoretical standards as before with structural parameters taken from Tables I and II. The only adjusted parameters were S_0^2 and energy shift ΔE_0 . The amplitude of the complex Fourier transform of the fluorescence EXAFS spectrum and corresponding fitting curve are presented in Fig. 6(a). As can be seen, the fitting curve describes well the first coordination shell and is in reasonable agreement with experimental data for the second coordination shell. Some disagreement between the fitting data and the EXAFS experiment for the second shell can be explained by the fact that, in our consideration, we ignore multiple-scattering paths contributing to EXAFS signal. In addition, in Fig. 6(b) we also show the comparison of the experimental EXAFS spectrum with the site-averaged spectrum calculated by using refined site-specific spectra of Fig. 3.

VI. DISCUSSION

We focus on two important findings. First, we note a significant increase in the Mn(A)-O first shell bond distance relative to the corresponding value for Fe(A)-O but almost no change in the bond distances for the B site. Second, perhaps, the most intriguing result of the DAFS analysis is the

TABLE II. Best-fit structural parameters for the B-site in MnFe_2O_4 artificial films obtained by fitting refined DAFS data.

Bond	N	R (Å)	σ^2 (10^{-3} Å ²)
B-O	3.1 ± 1	2.07 ± 0.01	1.2 ± 1.0
B-B	6.6 ± 1	3.02 ± 0.02	3.6 ± 1.0

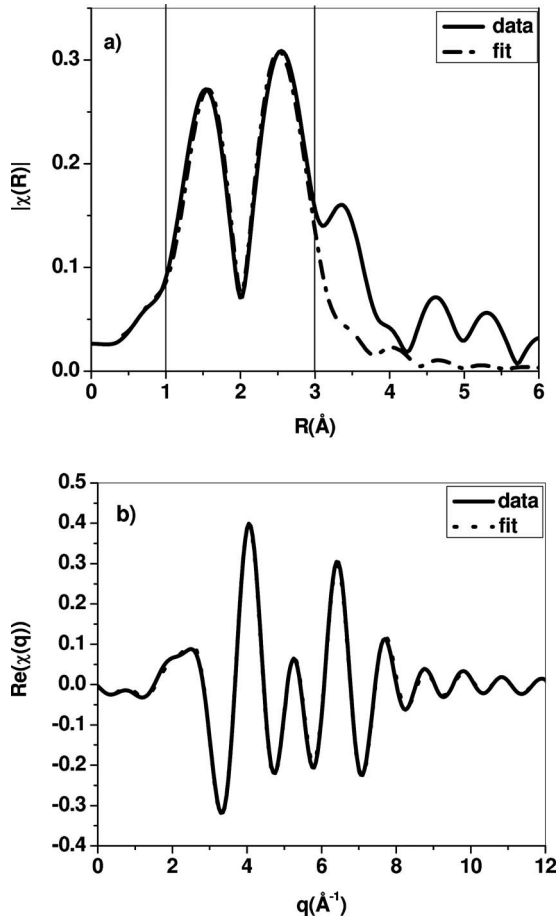


FIG. 5. (a) Magnitude of the complex Fourier transform of refined absorption data and its fit with FEFF6 theory for Mn absorbing atoms located at B sites. Vertical lines indicate fitting range. (b) Back Fourier transform of the fitted regions of R space and corresponding fit for Mn absorbing atoms located at B sites.

drastic reduction in the B-site effective coordination number observed for the first oxygen shell. A majority of Mn cations (about 80%) reside at A sites, while a minority (about 20%) occupy B sites. The observed expansion of the Mn(A)-O bonding distance can be easily predicted because the ionic radius of Mn is larger than that of Fe.³⁹ Based on atomic radii arguments, an expansion of Mn(B)-O bond distance compared to Fe(B)-O is also expected but not observed. In order to satisfy the bond-valence sum rule (see, for example, Ref. 40 and references therein), this reduction in the Mn(B)-O bonding distance should follow a corresponding reduction in coordination and/or change in valence. We suggest that the bonding distance of Mn(B)-sites is a result of two competing mechanisms: an expansion, due to larger ionic radii, and contraction, due to the reduced coordination. The similar chemical shifts in the absorption threshold between Mn(A) and Mn(B) sites as seen in Fig. 3(a) (≤ 1 eV) indicate that the valences at Mn(A) and Mn(B) sites are comparable. This, in turn, implies a larger degree of covalency for the Mn(B)-O bonding. We speculate that the anomalous magnetic properties obtained by varying the Mn content at B sites in artificial manganese ferrite films^{6,7} may be related to this unusual bonding and corresponding change in exchange

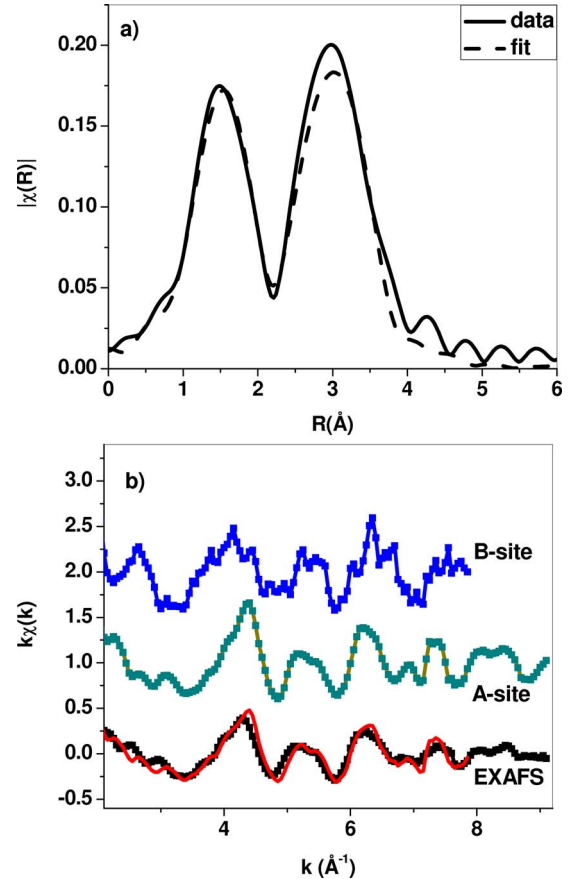


FIG. 6. (Color online) (a) Magnitude of the complex Fourier transform of experimental fluorescence EXAFS data and its fit with FEFF6 theory and site-specific structural parameters taken from DAFS analysis. The electron amplitude reduction factor obtained from the fit is $S_0^2=0.76$. (b) Refined site-specific absorption spectra together with experimental fluorescence EXAFS spectrum (points), reduced to photoelectron wave-vector space. In the solid line is shown the average of the site-specific spectra taken with corresponding site occupancies of 0.82 for the A site and 0.18 for the B site. The curves are shifted in the vertical scale for convenience.

coupling constants due to increased exchange integrals. This is also consistent with a relatively small MSD value for this bond. Finally, we note that our results pertain to manganese ferrite films grown under nonequilibrium conditions. The reduced coordination for B sites can be due to a nonequilibrium film growth technique. The point is that the film was grown with layer-by-layer growth under reduced substrate temperature. It is possible that such a growth technique may lead to producing additional vacancies and defects in the system. While it is likely that the findings here may also apply to bulk material, experiments on bulk single crystals are needed to corroborate the intrinsic nature of our results.

VII. CONCLUSIONS

Site-specific Mn local structure in manganese ferrite films was determined with DAFS spectroscopy. The DAFS data

analysis done with an iterative Kramers-Krönig algorithm made it possible to solve separately the local structure around different inequivalent Mn sites in the unit cell. We provided direct experimental evidence for Mn(A)-O bond distance being significantly increased relative to the Fe(A)-O distance.⁷ We demonstrated that DAFS spectroscopy is able to resolve the local atomic environment of Mn atoms at B sites and found a significant reduction in their first coordination shell number. This is consistent with the well-known tendency of Mn to be tetrahedrally coordinated in these compounds. The reliability of the data treatment was checked carefully, and we showed that the site-specific structural pa-

rameters obtained with DAFS allow us to describe fluorescence EXAFS spectrum independently.

ACKNOWLEDGMENTS

Work at Argonne was supported by the U.S. DOE, Office of Science, under Contract No. W-31-109-ENG-38. This research was also supported, in part, by National Science Foundation (NSF) Project No. DMR-022654 and by Office of Naval Research (ONR) Project No. N00014-01-1-0721. Authors acknowledge J. O. Cross and M. Newville for useful discussions and J. Lang for help with the experiment.

- ¹R. Vautier and M. Paulus, *Landolt-Börnstein Numerical Data and Functional Relationships in Science and Technology, New Series* (Springer-Verlag, Berlin, 1970), Vol. III/4b.
- ²J. Smit and H. P. J. Wijn, *Ferrites* (Wiley, New York, 1959).
- ³V. A. M. Brabers, in *Handbook of Magnetic Materials* (Elsevier, New York, 1995), Vol. 8, p. 189.
- ⁴*International Tables for Crystallography*, 5th ed., edited by T. Hahn (Kluwer Academic Publishers, Boston, 2002), Vol. A, p. 696.
- ⁵K. E. Sickafus, J. M. Wills, and N. W. Grimes, *J. Am. Ceram. Soc.* **82**, 3279 (1999).
- ⁶X. Zuo, S.-D. Yoon, J. A. Christodoulides, V. G. Harris, and C. Vittoria, *Appl. Phys. Lett.* **87**, 152505 (2005).
- ⁷A. Yang, V. G. Harris, S. Calvin, X. Zuo, and C. Vittoria, *IEEE Trans. Magn.* **40**, 2802 (2004).
- ⁸X. Zuo, A. Yang, S.-D. Yoon, J. A. Christodoulides, V. G. Harris, and C. Vittoria, *J. Appl. Phys.* **97**, 10G103 (2005).
- ⁹R. E. Vandenberghe and E. de Grave, in *Mössbauer Spectroscopy Applied to Inorganic Chemistry* (Plenum, New York, 1989), Vol. 3, p. 59.
- ¹⁰T. Egami and S. Billinge, *Underneath the Bragg Peaks: Structural Analysis of Complex Materials* (Elsevier, Oxford, 2003).
- ¹¹D. E. Sayers, E. A. Stern, and F. W. Lytle, *Phys. Rev. Lett.* **27**, 1204 (1971).
- ¹²*X-Ray Absorption: Principles, Applications, Techniques of EXAFS, SEXAFS and XANES*, edited by D. C. Konigsberger and R. Prince (Wiley, New York, 1988).
- ¹³H. Stragier, J. O. Cross, J. J. Rehr, L. B. Sorensen, C. E. Bouldin, and J. C. Woicik, *Phys. Rev. Lett.* **69**, 3064 (1992).
- ¹⁴L. Sorensen, J. Cross, M. Newville, B. Ravel, J. Rehr, H. Stragier, C. Bouldin, and J. Woicik, in *Resonant Anomalous X-ray Scattering: Theory and Applications*, edited by G. Materlik, C. Sparks, and K. Fischer (North-Holland, Amsterdam, 1994).
- ¹⁵J. García and G. Subías, *J. Phys.: Condens. Matter* **16**, R145 (2004).
- ¹⁶A. I. Frenkel, J. O. Cross, D. M. Fanning, and I. K. Robinson, *J. Synchrotron Radiat.* **6**, 332 (1999).
- ¹⁷I. J. Pickering, M. Sansone, J. Marsch, and G. N. George, *J. Am. Ceram. Soc.* **115**, 6302 (1993).
- ¹⁸J.-L. Hodeau, V. Favre-Nicolin, S. Bos, H. Renevier, E. Lorenzo, and J.-F. Berar, *Chem. Rev. (Washington, D.C.)* **101**, 1843 (2001).
- ¹⁹J. O. Cross, M. Newville, J. J. Rehr, L. B. Sorensen, C. E. Bouldin, G. Watson, T. Gouder, G. H. Lander, and M. I. Bell, *Phys. Rev. B* **58**, 11215 (1998).
- ²⁰J. O. Cross, W. T. Elam, J. C. Woicik, and L. B. Sorensen, *J. Synchrotron Radiat.* **6**, 335 (1999).
- ²¹B. Ravel, C. E. Bouldin, H. Renevier, J.-L. Hodeau, and J.-F. Berar, *Phys. Rev. B* **60**, 778 (1999).
- ²²M. G. Proietti, H. Renevier, J. L. Hodeau, J. García, J. F. Béar, and P. Wolfers, *Phys. Rev. B* **59**, 5479 (1999).
- ²³O. Ersen, V. Pierron-Bohnes, M.-H. Tuilier, C. Pirri, L. Khouchaf, and M. Gailhanou, *Phys. Rev. B* **67**, 094116 (2003).
- ²⁴D. C. Meyer, K. Richter, P. Paufler, and G. Wagner, *Phys. Rev. B* **59**, 15253 (1999).
- ²⁵J. O. Cross, Ph.D. thesis, University of Washington, Seattle (1996).
- ²⁶R. Karim and C. Vittoria, *J. Magn. Magn. Mater.* **167**, 27 (1997).
- ²⁷Value measured by MTI Corp. at Richmond, California.
- ²⁸ $a_{\text{MgO}}=4.2112 \text{ \AA}$ from R. W. G. Wyckoff, *Crystal Structures*, 2nd ed. (Interscience, New York, 1963), Vol. 1, p. 88.
- ²⁹R. W. G. Wyckoff, *Crystal Structures*, 2nd ed. (Interscience, New York, 1965), Vol. 3, p. 79.
- ³⁰D. T. Cromer and D. Liberman, *J. Chem. Phys.* **53**, 1891 (1970).
- ³¹D. Haskel, J. C. Lang, Z. Islam, A. Cady, G. Srajer, M. van Veenendaal, and P. C. Canfield, *Phys. Rev. Lett.* **95**, 217207 (2005).
- ³²B. Gilbert, B. H. Frazer, A. Belz, P. G. Conrad, K. H. Nealson, D. Haskel, J. C. Lang, G. Srajer, and G. De Stasio, *J. Chem. Phys.* **107**, 2839 (2003).
- ³³F. Farges, *Phys. Rev. B* **71**, 155109 (2005).
- ³⁴P. Glatzel, J. Yano, U. Bergmann, H. Visser, J. H. Robblee, W. Gu, F. M. F. de Groot, S. P. Cramer, and V. K. Yachandra, *J. Phys. Chem. Solids* **66**, 2163 (2005).
- ³⁵B. Ravel and M. Newville, *J. Synchrotron Radiat.* **12**, 537 (2005).
- ³⁶S. I. Zabinsky, J. J. Rehr, A. Ankudinov, R. C. Albers, and M. J. Eller, *Phys. Rev. B* **52**, 2995 (1995).
- ³⁷G. Subías, J. García, and J. Blasco, *Phys. Rev. B* **71**, 155103 (2005).
- ³⁸D. Haskel, J. W. Freeland, J. Cross, R. Winarski, M. Newville, and F. Hellman, *Phys. Rev. B* **67**, 115207 (2003).
- ³⁹R. D. Shannon, *Acta Crystallogr., Sect. A: Cryst. Phys., Diffr., Theor. Gen. Crystallogr.* **32**, 751 (1976).
- ⁴⁰I. D. Brown, *Acta Crystallogr., Sect. B: Struct. Sci.* **48**, 553 (1992).